Simulation of fluid-driven ruptures on pre-existing discontinuities in impermeable rocks

Brice Lecampion*, Ankit Gupta, Alexis Sáez, Regina Fakhretdinova, Antareep Sarma, Sylvain Brisson
Geo-Energy Lab - Gaznat Chair - EPFL
EPFL-ENAC-IIC-GEL, station 18, Lausanne CH-1015

November 2, 2024

Contents

1 Introduction **2**

2 Problem formulation **2**
2.1 Behavior of the rock matrix . . . 2
2.2 Hydro-mechanical behavior of discontinuities: fractures & faults . . . 4
2.2.1 Fluid flow . . . 4
2.2.2 A poroelasto-plastic interface law . . . 4
2.2.3 Interface yield criteria, flow rule, and damage . . . 6
2.2.4 Evolution of the interface permeability . . . 9

3 Numerical scheme **10**
3.1 Solid mechanics . . . 10
3.1.1 Elasto-plastic solver . . . 13
3.2 Fluid-flow in the discontinuities . . . 13
3.3 A fully-coupled hydro-mechanical solver . . . 14
3.3.1 Solution of the Jacobian system . . . 15
3.4 Adaptive time-stepping . . . 16

A Integration of the interface law **20**
A.1 Elastic predictor / plastic corrector scheme for a Mohr-Coulomb interface . . . 20
A.1.1 Trial elastic state . . . 20
A.1.2 Plastic correction . . . 20
A.2 Consistent tangent operator . . . 22
A.2.1 Consistent linearization . . . 22
A.2.2 In 2D
22
A.2.3 In 3D . . . 23
A.3 Tensile failure . . . 23

*Corresponding author

1 Introduction

This report aims to outline i) the mathematical formulation chosen to simulate hydraulic stimulation of a naturally fractured rock mass and ii) its numerical implementation. We assume from the onset that the rock matrix can be approximated by an elastic behavior and that all the inelastic deformations are localized along fractures. The model aims at simulating the shear an opening failure of pre-existing discontinuities in a material having uniform elastic properties. In this contribution, we will restrict to the case of an "impermeable" rock matrix over the time-scales of injection such that all the fluid flow occurs within the fractures - a limit often encountered in practical applications. This choice allows us to highly more explicitely some of the important features of the fluid-driven problem.

Notation

We use a Cartesian frame throughout defined by the basis vector $\boldsymbol{e}_i$, $i = 1, 2, 3$. We denote $\boldsymbol{x} = x_i \boldsymbol{e}_i$ ($\boldsymbol{y} = y_i \boldsymbol{e}_i$) as the coordinates vector. For convenience, we either use indices notation (with the usual summation convention over repeated indices), e.g. denoting σ_{ij} for the stress tensor, or bold-face for tensor and vectors. Similarly, either subscripts comma, e.g. $f_{,i} = \partial f / \partial x_i$, or operator, $\boldsymbol{\nabla} f = \partial f / \partial x_i \boldsymbol{e}_i$, notation are used for spatial derivatives. The use being clear depending on the context. We refer to time as t and write the time-derivative of f explicitely as $\dfrac{\partial f}{\partial t}$ or alternatively as $\dot{f}$ for short.

2 Problem formulation

Accounting for an initial stress state σ^o_{ij} in equilibrium with gravity and far-field tectonic loads, the quasi-static balance of momentum of the rock mass can be re-written as follows (in the absence of additional body forces):

$$\sigma_{ij,j} - \sigma^o_{ij,j} = 0 \qquad \text{in } \Omega \tag{1}$$

$$T_i = \sigma_{ij} n_j = T^g_i \qquad \text{on } \Gamma_{T_i} \tag{2}$$

$$u_i = u^g_i \qquad \text{on } \Gamma_{u_i} \tag{3}$$

$$\Gamma_{u_i} \cap \Gamma_{T_i} = \emptyset \qquad \Gamma_{u_i} \cup \Gamma_{T_i} = \Gamma \tag{4}$$

where Γ denotes the overall boundaries of the domain, Γ_{u_i} and Γ_{T_i} are the non-intersecting parts of the solid boundary where the displacement, respectively the tractions are imposed. We will distinguish between the pre-existing fracture(s) boundaries Γ_f in the inner part of the domain and the outer domain boundaries $\Gamma_{\partial\Omega}$ (which possibly extend to infinity), such that $\Gamma = \Gamma_f \cup \Gamma_{\partial\Omega}$. $T_i = \sigma_{ij} n_j$ denotes the traction acting on a facet of normal n_i.

We focus on problems driven by fluid injection at a specific location either under a given volumetric flow rate or controlled in terms of fluid over-pressure (above the hydrostatic). The associated pore-fluid pressurization will trigger ruptures on pre-existing discontinuities - either via shear failure or/and tensile failure of these discontinuities.

2.1 Behavior of the rock matrix

We assume that all the non-linearities will occur on the pre-existing discontinuities while the rock matrix behaves linearly (with its pore-space saturated with fluid). The constitutive relation (including pre-stress and initial pore-pressure) for a linearly isotropic porous solid matrix can be written in terms of stress (σ_{ij}) - strain (ϵ_{ij}), pore-pressure (p) and porosity (ϕ) changes as [Coussy, 2004]:

$$\sigma_{ij} - \sigma^o_{ij} = 2G\epsilon_{ij} + \frac{2G\nu}{1-2\nu}\epsilon_{kk}\delta_{ij} - \alpha(p - p^o)\delta_{ij} \tag{5}$$

$$\varphi = \phi - \phi^o = \alpha\epsilon_{kk} + \frac{p - p^o}{N} \tag{6}$$

where G and ν are the drained shear modulus and Poisson's ratio of the porous solid, α is the Biot's coefficient and N the intrinsic Biot modulus. The superscript ^{o} denotes the value in the initial reference state. The

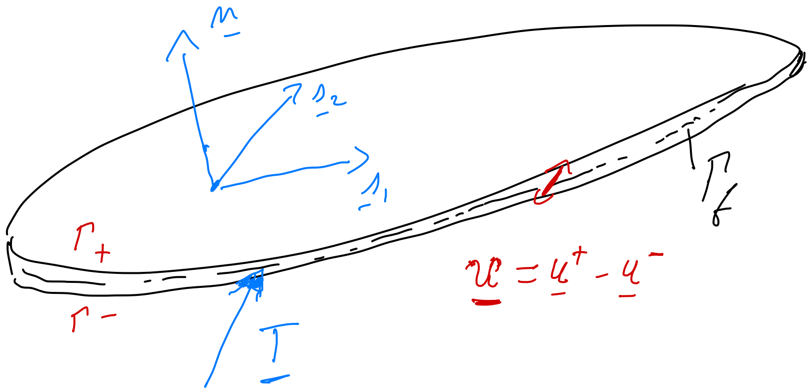

Figure 1: Definition of the local cartesian frame along a discontinuity $(\boldsymbol{s}_1, \boldsymbol{s}_2, \boldsymbol{n})$, traction and displacement discontinuity vectors.

fluid mass per unit of volume of porous media $m_f = \rho_f \phi$ can change due to porosity and fluid density variations. Defining the variation of fluid content as $\zeta = (m_f - m_f^o)/\rho_f^o$, for a fluid compressibility β_f, linear poroelasticity entails the following constitutive relation:

$$\zeta = (m_f - m_f^o)/\rho_f^o = (\phi - \phi^o) + \beta_f \phi^o (p - p^o) = \alpha \epsilon_{kk} + \frac{p - p^o}{M} \tag{7}$$

where the inverse of the Biot's modulus $1/M$ is the sum of the pore mechanical $(1/N)$ and fluid $(\phi^o \beta_f)$ compressibilities. The conservation of pore-fluid mass per unit of volume of porous media m_f reduces to first order for a compressible fluid to the following volume continuity equation (see e.g.Rice and Cleary [1976], Detournay and Cheng [1993], Coussy [2004]):

$$\frac{1}{\rho_f^o} \frac{\partial m_f}{\partial t} + q_{i,i} = \gamma \tag{8}$$

where γ is a source term and q_i is the fluid discharge vector given by Darcy's law (Darcy's velocity):

$$q_i = -\frac{k}{\mu_f} (p_{,i} - \rho_f g_i) \tag{9}$$

where k, μ_f, and ρ_f denote the intrinsic permeability of the porous solid, fluid viscosity, and density respectively. g_i is the Earth's gravity vector.

We *solely* focus our discussion on the limiting case where the rock matrix can be considered impermeable at the scale of the duration of the fluid injection. This limit is commonly encountered in practical engineering applications, as fractures typically have a permeability much larger than the rock matrix. In this limit, matrix poroelasticity reduces to an elastic problem with undrained properties, i.e. the bulk elastic moduli K is simply replaced by $K + \alpha^2 M$ (as the variation of fluid content is null in the rock matrix, such that (7) reduces to $(p - p_o) = -M\alpha\epsilon_{kk}$. The restriction to the case of an impermeable matrix allows to focus on the important aspects associated with non-linearities of fluid flow in the discontinuities and the associated numerical difficulties. It also stems from the fact that the semi-analytical solutions for fluid-driven ruptures that have been derived in recent years are restricted to such a case of an impermeable rock matrix. For tensile rupture (hydraulic fractures), some existing solutions account in a simplified manner fracture-matrix fluid exchange via early-time approximation (via the so-called Carter's leak-off model for example). In the remaining of this paper, the matrix is assumed impermeable/elastic for simplicity, with elastic properties G and ν.

2.2 Hydro-mechanical behavior of discontinuities: fractures & faults

Recognizing that the rock joints, fractures as well as faults can be considered at the macroscopic scale of interest as pre-existing discontinuities. We model them at macroscopic scale as zero thickness interface but recognize at the microscopic scale their non-zero thickness w notably to in relation to fluid flow. We use interchangeably the term interfaces, fracture, faults or discontinuity throughout.

For a discontinuity with a local normal $\boldsymbol{n}$, we define locally at any point along the discontinuity, an orthonormal Cartesian frame defined by the unit vectors (see Fig.1) $(\boldsymbol{s}_1, \boldsymbol{s}_2, \boldsymbol{n})$ where $\boldsymbol{s}_1$ and $\boldsymbol{s}_2$ define a 2D frame in-plane of the interface (locally tangent to the interface). We thus write the traction and displacement discontinuity vectors in this local frame as

$$\boldsymbol{T} = T_{s_1}\boldsymbol{s}_1 + T_{s_2}\boldsymbol{s}_2 + T_n\boldsymbol{n}$$
$$\mathbf{u} = \boldsymbol{u}^+ - \boldsymbol{u}^- = \mathrm{u}_{s_1}\boldsymbol{s}_1 + \mathrm{u}_{s_2}\boldsymbol{s}_2 + \mathrm{u}_n\boldsymbol{n}$$

where the n and s subscript therfore corresponds to the normal and shear components.

In view of their slenderness, fractures and faults are self-equilibrated, such that the action-reaction law apply (the traction vector vector is continuous across the discontinuity):

$$T_i^+ + T_i^- = (\sigma_{ij}^+ - \sigma_{ij}^-)n_j^+ = 0 \tag{10}$$

where the positive and negative superscript denote the relative sides of the interface (see Fig.1).

2.2.1 Fluid flow

The main difference between a bare fracture and a fault resides in the presence of gouge materials in the latter (see Fig. 2). We model a fault as an interface where slip is localized in a principal slip zone, but where fluid flow takes place over a zone of larger thickness. Bare fractures on the other hand, although having asperities at micro-scale, hold fluid flow strictly within the displacement discontinuity locus. Of course, a wide range of configurations exist between these two limits. A similar modeling framework holds for both cases pending the use of adequate models for the evolution of permeability, and proper constitutive parameters.

Denoting w as the thickness of the interface over which fluid flow occurs, the width integrated fluid mass balance (8) reads:

$$\frac{1}{\rho_f^o}\frac{\partial w m_f}{\partial t} + \nabla_{||} \cdot (w\boldsymbol{q}_{||}) + q_\perp^+ + q_\perp^- = w\gamma \tag{11}$$

$$\boldsymbol{q}_{||} = -\frac{k}{\mu_f}\left(\boldsymbol{\nabla}_{||}p - \rho_f\boldsymbol{g}_{||}\right) \tag{12}$$

where the subscript $||$ restricts the component of vectors and differential operators to the coordinates in the fracture mid-plane. More precisely, the along the fracture fluid discharge $q_{||}$ corresponds to the width-averaged Darcy's fluid velocity. For quiescent initial conditions ($\boldsymbol{q}_{||}(t=0) = \mathbf{0}$), the initial pore-pressure p^o is hydrostatic such that $\boldsymbol{\nabla}_{||}p^o = \rho_f\boldsymbol{g}_{||}$, such that Darcy's law can be re-expressed as function of the over-pressure above hydro-static $p - p^o$: $\boldsymbol{q}_{||} = -\frac{k}{\mu_f}\boldsymbol{\nabla}_{||}(p - p^o)$.

The leak-off velocities from the upper $q_\perp^+$ and $q_\perp^-$ account for fluid exchange with the rock matrix. It can be accounted for by directly coupling the interface and matrix flow explicitly [Berre et al., 2019] or in the view of the short time-span of fluid injection via approximate 1D diffusion models in the matrix in a direction perpendicular to the discontinuity [Kanin et al., 2019, 2020]. In what follows, we focus on the impermeable case, and drop the fluid exchange between the rock and the matrix for clarity.

2.2.2 A poroelasto-plastic interface law

We model faults and fracture as zero thichkness poroelastoplastic interfaces. For a pre-existing discontinuity such as rock joints, a large number of models [Gens et al., 1990, Carol et al., 1997] introduces a split between an elastic part of the displacement discontinuity (controlled by interface stifnesses) and a 'sliding'/ 'opening' part activated when the traction reaches a frictional yield limit. Such a 'sliding'/ 'opening' part of the

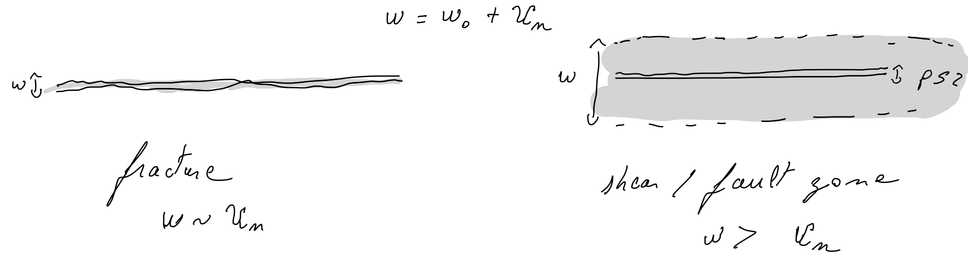

Figure 2: Differences between a fracture (left) and a fault/shear zone (right) with a principal slip zone. Fluid flow can occurs over a larger thickness than any induced dilation of the principal slip zone for a fault. On the contrary, for a fracture, flow is mostly restricted to the locus of the displacement discontinuity.

displacement discontinuity is sometimes referred to as plastic, following the classical terminology of elasto-plasticity, although it can be reversible via reversal of the loads. It is more accurate to refer to inelastic or crack like displacement discontinuity for the interface. An "elasto-plastic" like formalism (also accounting for damage) allows to properly modeled the deformation of rock joints, accounting for the important effect of variable dilatancy via the use of a non-associated flow rule. Such formalism is very similar to cohesive zone models (CZM) of fracture [Park and Paulino, 2011], although the interface stiffness is in reality for rock not a mere penalty parameter but allows to properly model the non-linearity of contact closure.

We decompose the displacement discontinuity vector across the interface in an elastic $\mathfrak{u}_i^e$ (reversible) and inelastic / crack-like $\mathfrak{u}_i^p$ part:

$$\mathfrak{u}_i = \mathfrak{u}_i^e + \mathfrak{u}_i^p. \tag{13}$$

The variation of porosity $\phi - \phi^o = \varphi$ is split in a similar fashion ($\varphi = \varphi^e + \varphi^p$). The increment of plastic/inelastic work of the interface (of thichkness w) is thus: $\mathrm{d}W^p = T_i \mathrm{d}\mathfrak{u}_i^p + p\mathrm{d}(w\varphi^p)$. Like for all geomaterials, the variation of plastic porosity is equal to the plastic volumetric strain as the solid constituents are plastically incompressible in comparison to the grain re-arrangements leading to porosity changes. For an interface, this translates to $\mathfrak{u}_n^p = w\varphi^p$. We therefore obtain that the increment of plastic work is a function of the Terzaghi's effective tractions $\boldsymbol{T}' = \boldsymbol{T} + p\boldsymbol{n}$:

$$\mathrm{d}W^p = (T_i + p\, n_i)\mathrm{d}\mathfrak{u}_i^p = T_i' \mathrm{d}\mathfrak{u}_i^p. \tag{14}$$

All experimental observations in geomaterial (matrix and discontinuities) confirm that Terzaghi effective stress drives inelastic deformation both for matrix and interface inelastic deformation.

Accounting for inelastic displacement discontinuity, upon integration over the width w, the poroelasto-plastic constitutive relation of the interface can be expressed in terms of the traction $\boldsymbol{T}$ and the elastic part of the displacement discontinuity vector $\boldsymbol{\mathfrak{u}}^e = \boldsymbol{\mathfrak{u}} - \boldsymbol{\mathfrak{u}}^p$:

$$\boldsymbol{T} - \boldsymbol{T}^o = \mathbb{C} \cdot (\boldsymbol{\mathfrak{u}} - \boldsymbol{\mathfrak{u}}^p) - \alpha(p - p^o)\boldsymbol{n} \tag{15}$$

$$\varphi - \varphi^p = \alpha \frac{(\mathfrak{u}_n - \mathfrak{u}_n^p)}{w} + \frac{p - p^o}{N} \tag{16}$$

In the previous constitutive relation, $\mathbb{C}$ denotes the interface stiffness matrix (in N/m) which is possibly non-linear (as function of the Terzaghi's effective tractions). In the local cartesian reference frame of the interface, assuming an isotropic behavior, $\mathbb{C}$ is written as function of a normal K_n and shear K_s stiffness:

$$\mathbb{C} = K_s \left(\boldsymbol{s}_1 \otimes \boldsymbol{s}_1 + \boldsymbol{s}_2 \otimes \boldsymbol{s}_2 \right) + K_n \boldsymbol{n} \otimes \boldsymbol{n} \tag{17}$$

For usual 'filling' materials inside the discontinuity (granular gouge or/and asperities), the porous skeleton is much more compliant than its solid constituents such that the Biot's coefficient of the interface reduce to unity: $\alpha = 1$ [Detournay and Cheng, 1993, Coussy, 2004]. As a result, like for soils, the Biot's and Terzaghi's effective tractions coincides (the former strictly governing the poroelastic deformation while the later drives plastic deformation - see Coussy [2004] for discussion). In this limit, the intrinsic Biot pore compressibility $1/N$ is usually negligible compared to the fluid compressibility. We assume $\alpha = 1$, and keep the possibility of non-zero pore compressibility of the filling material. It is also important to note that if the interface/fracture fails in tension, upon full opening, the shear and normal stiffnesses of the interface vanishes as discussed in the next subsections.

After re-arranging (13)-(16) with the previous assumptions, the constitutive relations of the poroelasto-plastic interface can be written as:

$$\boldsymbol{T}' - \boldsymbol{T}'^{\,o} = \mathbb{C} \cdot (\mathfrak{u} - \mathfrak{u}^p) \tag{18}$$

$$w\varphi = \mathfrak{u}_n + \frac{w}{N}(p - p^o) \tag{19}$$

The width integrated variation of fluid content of the interface is $w(m_f - m_f^o)/\rho_f^o = w\varphi + w\phi^o\beta_f(p - p^o)$. Note that the interface width w is the sum of an initial thickness w^o and the normal displacement discontinuity: $w = w^o + \mathfrak{u}_n$.

The integrated fluid conservation (11) can thus be rewritten as

$$\frac{\partial \mathfrak{u}_n}{\partial t} + \frac{w}{M}\frac{\partial p}{\partial t} + \nabla_{||} \cdot (w\boldsymbol{q}_{||}) + q_{\perp}^{+} + q_{\perp}^{-} = w\gamma \tag{20}$$

with $1/M = 1/N + \phi^o\beta_f$ the Biot's modulus of the porous interface.

2.2.3 Interface yield criteria, flow rule, and damage

Inelastic displacement discontinuity occur when a yield criteria written in term of the effective tractions acting on the interface is reached. Besides effective tractions, the yield criteria may also depend on one or more internal variables $\boldsymbol{\chi}$ tracking the internal state of the interface (such as the cumulated plastic shear slip). Denoting $F(\boldsymbol{T}', \boldsymbol{\chi})$ the yield function, sole elastic deformation occur when $F(\boldsymbol{T}', \boldsymbol{\chi}) < 0$, while the constraint $F(\boldsymbol{T}', \boldsymbol{\chi}) = 0$ is active upon plastic yielding.

To capture with the simplest possible model, most of the mechanisms observed experimentally for rock joints and fractures [Barton, 1976, Barton et al., 1985], we combine a Mohr-Coulomb yield surface with a tensile cut-off and allow for the weakening of cohesion, friction and tensile strength. The combination of these two distinct criteria notably allows to simulate the observed difference in both shear and tensile fracture of rock joints. A non-associated plastic flow rule is used for the plastic displacement related to Mohr-Coulomb to properly model shear-induced dilatancy and the transition to a critical state, while an associated flow rule is used for the tensile cut-off. Other choice of constitutive models is of course possible - see Gens et al. [1990], Carol et al. [1997], Mroz and Giambanco [1996], Stupkiewicz and Mroz [2001], Son et al. [2004], Zandarin et al. [2013], Li et al. [2016, 2020] among others.

In the local frame of reference of the interface, it is useful to introduce the shear component of the effective traction $\boldsymbol{\tau}$ and the principal shear direction vector $\hat{\boldsymbol{s}}$:

$$\boldsymbol{\tau} = T'_{s_1}\boldsymbol{s}_1 + T'_{s_2}\boldsymbol{s}_2 = \|\boldsymbol{\tau}\|\hat{\boldsymbol{s}} \qquad \hat{\boldsymbol{s}} = \frac{\boldsymbol{\tau}}{\|\boldsymbol{\tau}\|} \qquad \|\hat{\boldsymbol{s}}\| = 1 \qquad \boldsymbol{\tau} \cdot \hat{\boldsymbol{s}} = \|\boldsymbol{\tau}\| \tag{21}$$

$\hat{\boldsymbol{s}}$ is an unit vector indicating the principal direction of shear, of course we have $\boldsymbol{n} \cdot \hat{\boldsymbol{s}} = 0$ and

$$\boldsymbol{T}' = \boldsymbol{\tau} + T'_n\boldsymbol{n}.$$

Similarly, we define the shear slip vector as

$$\boldsymbol{\delta} = \mathfrak{u}_{s_1}\boldsymbol{s}_1 + \mathfrak{u}_{s_2}\boldsymbol{s}_2$$

such that the displacement discontinuity vector is $\mathfrak{u} = \boldsymbol{\delta} + \mathfrak{u}_n\boldsymbol{n}$. We track the state of the interface with two distinct internal variables $\boldsymbol{\chi} = (\chi_t, \chi_s)$:

1. The maximum accumulated total inelastic displacement discontinuity magnitude

$$\chi_t = \max(\|\mathfrak{u}^p(t)\|)$$

to model the evolution of cohesion and tensile strength,

2. the maximum accumulated inelastic shear slip displacement discontinuity magnitude

$$\chi_s = \max(\|\boldsymbol{\delta}^p(t)\|)$$

to model the evolution of the friction and dilation coefficient of the discontinuity.

Mohr-Coulomb failure

The Mohr-Coulomb yield function for an interface is given by

$$F_{mc}(\boldsymbol{T}', \boldsymbol{\chi}) = \|\boldsymbol{\tau}\| - f(\chi_s)T'_n - C(\chi_n) = \boldsymbol{T}' \cdot \hat{\boldsymbol{s}} - f(\chi_s)\boldsymbol{T}' \cdot \boldsymbol{n} - C(\chi_n)$$

Upon reaching this frictional yield limit, inelastic variation of displacement discontinuity occurs according to a non-associated flow rule:

$$\begin{aligned} F_{mc}(\boldsymbol{T}', \boldsymbol{\chi}) &< 0 \qquad \dot{\mathbf{u}}^p = 0 \\ F_{mc}(\boldsymbol{T}', \boldsymbol{\chi}) &= 0 \qquad \dot{\mathbf{u}}^p = \dot{\lambda} \boldsymbol{\nabla}_{\boldsymbol{T}'} G \qquad \dot{\lambda} > 0 \end{aligned}$$

where a dot $\dot{\square}$ denotes the time-derivative. $G(\boldsymbol{T}', \boldsymbol{\chi})$ is a non-associated inelastic flow potential taken here as

$$G(\boldsymbol{T}, \boldsymbol{\chi}) = \|\boldsymbol{\tau}\| + \psi(\chi_s)T'_n$$

where $\psi \geq 0$ is a dilatancy coefficient which evolves as function of the internal variable controlling the evolution of friction. The dilatancy coefficient decreases as inelastic slip accumulates such that the interface eventually reaches a criticial state where no inelastic dilation occur, i.e. $\lim_{\chi_s \to \infty} \psi = 0$.

The inequality related to the activation of the yield criteria and the inelastic deformation has the following complementary Karush-Kuhn-Tucker condition

$$\dot{\lambda} F_{mc} = 0$$

which reflect the fact that if $F_{mc} < 0$, $\dot{\lambda} = 0$ no inelastic displacement discontinuity occur while if $\dot{\lambda} > 0$ then the yield function must be satisfied $F = 0$. The gradient of F_{mc} and G with respect to the effective traction $\boldsymbol{T}'$ are chiefly obtained as:

$$\begin{aligned} \boldsymbol{\nabla}_{\boldsymbol{T}'} F_{mc} &= \frac{\boldsymbol{\tau}}{\|\boldsymbol{\tau}\|} + f(\chi_s)\boldsymbol{n} = \hat{\boldsymbol{s}} + f(\boldsymbol{\chi})\boldsymbol{n} \\ \boldsymbol{\nabla}_{\boldsymbol{T}'} G &= \hat{\boldsymbol{s}} + \psi(\chi_s)\boldsymbol{n} = \boldsymbol{N}(\boldsymbol{T}') \end{aligned}$$

such that the non-associated Mohr-Coulomb inelastic flow rule can be re-written as:

$$F_{mc}(\boldsymbol{T}', \boldsymbol{\chi}) = 0 \qquad \dot{\mathbf{u}}^p = \dot{\lambda}(\hat{\boldsymbol{s}} + \psi(\chi_s)\boldsymbol{n}) \qquad \dot{\lambda} > 0.$$

The plastic multiplier $\dot{\lambda}$ is function of the global equilibrium and locally obtained from the condition that during an inelastic evolution, the state of effective tractions must remain on the yield surface, in other words when $\dot{\lambda} > 0$, we must have

$$\dot{F}_{mc} = \boldsymbol{\nabla}_{\boldsymbol{T}'} F_{mc} \cdot \dot{\boldsymbol{T}}' + \boldsymbol{\nabla}_{\boldsymbol{\chi}} F_{mc} \cdot \dot{\boldsymbol{\chi}} = 0$$

which is referred to as the consistency condition in the theory of elasto-plasticity.

Evolution of friction, dilatancy and cohesion

The friction and dilation coefficients are taken function of the maximum accumulated inelastic shear displacement discontinuity χ_s. The friction and dilation coefficients are assumed to vary from an initial value f_p (respectively ψ_p) to a residual value f_r (respectively to $\psi_r = 0$ - reproducing the fact that frictional sliding ultimately reaches a critical state without any more dilation). We write the following evolution

$$\begin{aligned} f(\chi_s) &= (f_p - f_r)\, W(\chi_s/d_c) + f_r \\ \psi(\chi_s) &= \psi_p \mathcal{W}(\chi_s/d_c) \end{aligned}$$

with $\mathcal{W}(x)$ a smooth function going from 1 (at $x = 0$) to zero (at $x \geq 1$). d_c is the critical slip weakening distance scale. The simplest choice for $\mathcal{W}$ is a linearly decreasing function between 0 and 1.

The cohesion is taken function of the maximum total accumulated inelastic displacement discontinuity χ_t. It typically decreases from a peak value c_p to zero over a critical distance of inelastic displacement discontinuity w_c:

$$c(\chi_t) = c_p \mathcal{W}(\chi_t/w_c).$$

Note that the critical opening distance w_c may be different than the critical slip distance d_c.

Tensile failure & contact

In addition to Mohr-Coulomb frictional failure with cohesion, we add a tensile cut-off to better capture the failure of fracture in tension (notably to simulate the creation of new fractures). The yield criteria in tension is simply expressed as:

$$F_t(\boldsymbol{T}', \boldsymbol{\chi}) = T'_n - \sigma_t(\chi_n) = \boldsymbol{T}' \cdot \boldsymbol{n} - \sigma_t(\chi_n) \leq 0. \tag{22}$$

The flow rule for such a pure tensile cut-off is

$$F_t(\boldsymbol{T}', \boldsymbol{\chi}) = 0 \qquad \dot{\mathfrak{u}}^p > 0 \tag{23}$$

with the complementary condition $F_t(\boldsymbol{T}', \boldsymbol{\chi})|\dot{\mathfrak{u}}^p| = 0$. The inelastic displacement discontinuity depends on the loading/unloading sequence from the application of the constraint $F_t(\boldsymbol{T}', \boldsymbol{\chi}) = 0$ in the solution of the global equilibrium.

The evolution/degradation of the tensile strength as function of the maximum encountered 'inelastic' displacement discontinuity χ_t is written similarly than for the evolution of cohesion:

$$\sigma_t(\chi_t = \max(\|\mathfrak{u}^p\|)) = \sigma_p \mathcal{W}(\chi_t / w_c)$$

with $\mathcal{W}$ a linearly decreasing function from 1 (when $\chi_t/w_c = 0$) to 0 at $\chi_t/w_c = 1$. If the yield criteria is satisfied $F_t(\boldsymbol{T}, \boldsymbol{\chi}) = 0$, neglecting the elasticity of the interface (rigid prior to yield case), we obtain a classical mode I traction-separation law between normal traction and opening of cohesive zone models.

We define a damage measure of the interface as $d = \min(\chi_t/w_c, 1)$. Upon full damage, when the tensile strength of the interface is now null, the elastic stiffness of the interface vanishes if the tensile failure criterion is active. In other words,

$$K_n = K_s = 0 \text{ if } F_t(\boldsymbol{T}', \chi_n \geq w_c) = 0 \tag{24}$$

If the interface opens as a crack (fully damaged), upon unloading, contact will occur. We model the fact that at micro-scale the created fracture exhibit a roughness by introducing a positive macroscopic inelastic residual width w_R. The Signorini contact conditions when the interface has a completely degraded tensile strength therefore reads:

$$\mathfrak{u}^p_n - w_R \geq 0 \qquad F_t(\boldsymbol{T}', \chi_n \geq w_c) \leq 0 \qquad (\mathfrak{u}^p_n - w_R) F_t(\boldsymbol{T}', \chi_n) = 0 \tag{25}$$

Under pure mode I loading, the residual width w_R upon full damage, is taken as a fraction of the critical width w_c: $w_R = \alpha w_c$ (with $\alpha \leq 1$).

We have written the contact condition as function of the inelastic part of the displacement discontinuity in order to ensure a positive total displacement discontinuity (no overlap) under compression. This is particularly important as the non-linearity of the interface flow properties are related to the normal component of the displacement discontinuity. It is important to note that for a pre-existing fractures $\sigma_p = 0$, we must have $w_R = 0$ ($w_c = 0$) in this formulation. This can be grasped by the following example. Assuming an initial normal compressive traction as $T'_n = -\sigma_o$, under pure tensile loading, the interface will open when the elastic normal opening (from the initial state) is $\mathfrak{u}^{e,o}_n = \sigma_o/K_n$. For such a pre-existing fracture that opens, upon unloading, contact starts when the total normal displacement discontinuity goes back to $\mathfrak{u}^{e,o}_n$ or alternatively when the inelastic part of the normal displacement discontinuity goes to zero, therefore indicating that $w_R = 0$ under pure mode I loading for pre-existing / fully broken / fractures.

Of course, the residual width w_R also evolves with inelatic shear-induced dilation under frictional failure due to shear loading. The evolution of the residual width w_R must therefore be written as:

$$w_R = \alpha w_c + \int_0^t \psi(\chi_s) \chi_s \, \mathrm{d}t \tag{26}$$

to account for the effect of shear-induced dilation in mixed mode loading. This notably allows to model the case where shear-induced dilation is followed by tensile opening and then closure.

Effective stress dependent stiffness

The interface stiffness are only active when the interface is not yielded in tension. Notably for pre-existing / fully broken fractures, these elastic stiffness are only active when the interface is under compression effective stresses. Although from a modeling perspective, a constant interface stiffness is the simplest choice, rock interface/joints exhibit a clear non-linear response upon closure [Bandis et al., 1983, Barton et al., 1985]. We settle either for a constant value of normal and shear stiffnesses or for the well-accepted hyperbolic model first proposed by Bandis et al. [1983] for the normal stiffness K_n. Such a phenomenological model - found adequate for rock joints - can be written as

$$K_n = K_i \left(1 - \frac{T_n'}{k_i v_m}\right)^2 \tag{27}$$

where K_i is the stiffness upon closure (at zero effective normal traction) and v_m is a characteristic closure distance. Note that $K_i v_m = \Sigma_m$ can be seen as a "characteristic closure" pressure: the stiffness is four times the initial value when $-T_n' = \Sigma_m$. For an interface with initially some tensile strength, one can account for the degradation of the normal stiffness due to tensile failure by decreasing the stiffness upon closure K_i as function of the interface damage $d = \min(\chi_t/w_c, 1)$, taking for example $K_i = K_* \exp(-\beta d)$ or other adequate functional forms.

A linear dependence of the tangent stiffness on the normal effective stress has also been found to be adequate in some cases [Bandis et al., 1983, Rutqvist and Stephansson, 2003]. For uncorrelated fracture, the closure relation is found to be logarithmic - see Bandis et al. [1983], and actually similar to well-known behavior of the contact mechanics of rough uncorrelated surfaces [Persson, 2007], and to the well-observed compaction relation of granular medium Mitchell et al. [2005]. In that case, the stiffness evolves linearly with $-T_n'$ [Cornet, 2015, Bandis et al., 1983]:

$$K_n = -\kappa T_n'$$

such that the elastic variation of normal displacement discontinuity under compressive normal stress is logarithmic

$$\dot{T}_n' = \kappa T_n' \dot{\mathfrak{u}}_n^{\,e} \rightarrow \mathfrak{u}_n = (1/\kappa) \log |T_n'|/|T_n'^{o}|$$

In comparison to the normal stiffness, the non-linearities of the shear stiffness k_s are not as well characterized. We settle for a constant value of K_s for simplicity. This has notably the advantage of simplifying the solution of the interface constitutive relation via the classical elastic-predictor plastic corrector scheme of elastoplasticity (see appendix A for details).

Selection of the failure mode and solution

When the yield criteria for both failure modes are reached, we select an unique active mode of failure based on a continuous function first proposed in [Itasca Consulting Group, 2010] as:

$$h(\boldsymbol{T}', \boldsymbol{\chi}) = \|\boldsymbol{\tau}\| - (c(\chi_n) - f(\chi_s)\sigma_t(\chi_n) + \alpha(\boldsymbol{\chi})(T_n' - \sigma_t(\chi_n))$$

with $\alpha(\boldsymbol{\chi}) = \sqrt{1 + f(\chi_s)^2} - f(\chi_s)$. If $h > 0$, shear failure is selected, otherwise tensile failure. The function h separates the domain where shear and tensile failure is active - see Fig. **??**.

The rate of change of effective tractions as function of the rate of change of the total displacement discontinuity of the interface is the solution of the previously described path-dependent non-linear elasto-plastic relations. The details of the integration of the interface consistitutive description chosen here are given in appendix A. Such a local interface relation along the pre-existing discontinuities, must of course be solved in conjunction with the global quasi-static elastic equilibrium of the whole fractured medium and the fluid-flow along the discontinuities as discussed in section 2.2.

2.2.4 Evolution of the interface permeability

In the formalism of coupled hydro-mechanics, for the case of closed fractures/joints (under compressive effective stress), the evolution of permeability are sometimes expressed in terms of the current effective normal traction in a similar way than for granular soils [Rice, 1992, ?]. This is however no longer the case when the fractures become open - for which the effective normal traction becomes zero. It is more convenient to express the variation of permeability as function of the variation of the interface aperture, or the variation of inelastic interface porosity (the two being equal in our formalism). More specifically, it is the change in interface conductivity kw that governs the resistance to flow in the interface as described by eqs.(11)-(12).

Flow in bare fracture: modified cubic law

For mechanically open fractures, the normal displacement discontinuity is larger than the initial width of the interface w_o: $w = w_o + \mathfrak{u}_n \approx \mathfrak{u}_n$ as $\mathfrak{u}_n \gg w_o$. In that case, Poiseuille law directly provides the corresponding hydraulic transmissibility as $kw = \mathfrak{u}_n^3/12$.

The formalism of the cubic law is also used for mechanically closed fractures (under compressive effective normal traction) [Witherspoon et al., 1980]. However, it is generalized by introducing a finite hydraulic width $\omega_o = f(w_o)$ in addition to the mechanical aperture. This allows to capture the deviation from the cubic law at large compressive loads for which the mechanical aperture reduces to zero. The cubic law is thus written as function of the "hydraulic aperture" $\omega = \omega_o + \mathfrak{u}_n$ to account for the fact that if initially closed, under significant compressive stress, the interface have a remaining permeability. We write

$$wk(\mathfrak{u}_n) = \frac{w(\omega_o + \mathfrak{u}_n)^2}{12} \qquad w = w_o + \mathfrak{u}_n \tag{28}$$

where $\mathfrak{u}_n$ is the normal component of the displacement discontinuity. In the reference configuration / initial state, it is necessarily equal to zero. This corresponds to the initial state for which the hydraulic transmissibility of the interface is $w_o\omega_o^2/12$. The initial hydraulic width ω_o may possibly be different than the initial interface thickness w_o, although for bare fracture we settle for $\omega_o = w_o$. A model that reproduces well experimental data for the flow in fractures under compression can be written as a

$$wk(\mathfrak{u}_n) = \frac{1}{12}\left(\mathfrak{u}_n \times (1 + \sigma_w/\mathfrak{u}_n)^{-3/2} + w_o\right)^3 \tag{29}$$

where σ_w is akin to a roughness scale that governs the transition between a constant hydraulic transmissibility at small mechanical apertures to the classical cubic law at large mechanical apertures. All the simulations reported in this paper assumes $\sigma_w = 0$ for simplicity.

Flow in fault/shear-zone

For the case of a thicker / mature fault zone, flow occurs within a unit containing a principal slip zone (see Fig.). It differs from the previouss case of a bare fracture. In a simple model, the flow across the entire thickness of the fault zone can be obtained by summing the flow within the group and the zone of localized displacement discontinuity (the principal slip zone). The overall hydraulic transmissivity of the "interface" can be written as:

$$kw = k_f(T_n')w_o + k_{psz}(\mathfrak{u}_n)\mathfrak{u}_n \tag{30}$$

where k_f is the permeability of the fault zone (which may be non-linear dependent on the effective normal stress), and k_{psz} is the permeability associated with the displacement discontinuity associated with the principal slip zone. For the latter, one can use the cubic law $k_{psz}(\mathfrak{u}_n)\mathfrak{u}_n = \mathfrak{u}_n^3/12$ for simplicity. The interface conductivity (with respect to the initial value) for bare fractures and a shear zone thus evolves in $(1+\mathfrak{u}_n/w_o)^3$ and $1 + (\mathfrak{u}_n/(k_g w_o)^{1/3})^3$ respectively (for a constant permeability for the fault zone).

3 Numerical scheme

We describe a fully-coupled implicit scheme for the solution of the time-dependent problem of fluid flow along the fractures/faults combined with the balance of linear momentum of the medium accounting for the non-linear constitutive relations of the fractures/faults previously described.

3.1 Solid mechanics

Recognizing that all the non-linearites lies on the interface/fractures, we use a collocation boundary element method for the discretization of the balance of momentum for the linearly elastic rock domain. In particular, we use a displacement discontinuity method and the traction hyper-singular boundary integral equation for linear isotropic quasi-static elasticity [Crouch and Starfield, 1983, Hills et al., 1996, Bonnet, 1999, Mogilevskaya, 2014]. The traction hypersingular boundary integral equation can be written as:

$$T_i(\boldsymbol{x}_*) - T_i^o(\boldsymbol{x}_*) = \lim_{\boldsymbol{x}\to\boldsymbol{x}_*} \int_\Gamma \left[\mathbb{T}_i^a(\boldsymbol{y},\boldsymbol{x})\left(T_a(\boldsymbol{y}) - T_a^o(\boldsymbol{y})\right) - \mathbb{H}_i^a(\mathbf{x},\mathbf{y})u_a(\boldsymbol{y})\right] \,\mathrm{d}S_y \\ - \lim_{\boldsymbol{x}\to\boldsymbol{x}_*} \int_{\Gamma_f} \mathbb{H}_i^a(\mathbf{x},\mathbf{y})\mathrm{u}_a(\boldsymbol{y}) \,\mathrm{d}S_y \tag{31}$$

where the fundamental elastic kernels appearing in this boundary integral equation are:

- $\mathbb{T}_i^a(\boldsymbol{x},\boldsymbol{y}) = S_{ij}^a(\boldsymbol{x},\boldsymbol{y})n_j$ the traction vector on a surface of normal $\boldsymbol{n}$ at $\boldsymbol{y}$ due to a unit point force in direction $\boldsymbol{e}_a$ located at $\boldsymbol{x}$ ($\mathbb{S}_{ij}^a$ denotes the corresponding stress field),
- $\mathbb{H}_i^a(\boldsymbol{y},\boldsymbol{x}){=}n_j(\mathbf{x})c_{ijkl}S_{ab,l}^k(\mathbf{y}{,}\mathbf{x})n_b(\mathbf{y})$ corresponds to the traction vector on a surface at $\boldsymbol{x}$ due to a dislocation dipole of normal $\boldsymbol{n}(\boldsymbol{y})$ and unit intensity located at $\boldsymbol{y}$. It is hyper-singular.

The boundary element method is particularly attractive to simulate injection at depth for which the domain of interest can be considered as infinite. In that case, the first integral in 31 as the outer boundary of the solid Γ goes to infinity. The problem reduces to a simple boundary integral equation between the traction and displacement discontinuity vector along the discontinuities. We discretize the different fractures / faults and assume a piece-wise constant approximation of the displacement discontinuity over a given element, and collocate the boundary integral equation at the centroid of each element in the mesh [Crouch and Starfield, 1983, Hills et al., 1996]. This choice simplify the treatment of the hyper-singular kernel. Notably, the integrals are evaluated before the limit is taken and as such remain regular. In particular, we use analytical integration of these integral as presented in Hills et al. [1996], Fata [2011], Nikolskiy et al. [2015] among many others. In what follow, we model either 2D plane-strain, axisymmetric or fully 3D configurations - using respectively segment and triangular surface elements for which these integrals are available analytically.

Rice [1993] introduced the concept of a quasi-dynamics boundary-integral equation and its use to model the faults by retaining only a local mass inertial term (associated with $\rho\,\ddot{\boldsymbol{u}}$) to capture in a simple form wave radiation during fast interface rupture. It can be obtained from the formulation of the full elastodynamics boundary integral equation. In fine, a local term $\boldsymbol{\eta}\cdot\dfrac{\partial\mathbf{u}(\boldsymbol{x},t)}{\partial t}$ is substracted to the quasi-static boundary integral operator, with

$$\boldsymbol{\eta} = \frac{1}{2}\begin{bmatrix} G/c_s & 0 & 0 \\ 0 & G/c_s & 0 \\ 0 & 0 & G/c_p \end{bmatrix}$$

where $c_s = \sqrt{\frac{G}{\rho}}$ and $c_p = \sqrt{\frac{K+4/3G}{\rho}}$ are the shear and compressional elastic waves speed of the material. It is important to note that such a quasi-dynamic term is active only at very large slip/opening rate, essentially only when an instability occurs in association to the weakening of the interface properties. It has merely no effects otherwise.

Final system Using a collocation displacement discontinuity method, the hypersingular boundary integral equations accounting for a quasi-dynamic term reduces to a dense linear system

$$\boldsymbol{T}(t) - \boldsymbol{T}^o(t) = \mathbb{E}\cdot\mathbf{u}(t) - \boldsymbol{\eta}\frac{\partial\mathbf{u}(t)}{\partial t} \tag{32}$$

where $\boldsymbol{T}$ is the vector of tractions at all collocation points in the mesh which evolves with time in response to fluid injection, $\boldsymbol{T}^o$ the vector of tractions at all collocation points due to far-field/initial in-situ stress (also possibly be time-dependent), and $\mathbf{u}$ the vector of all displacement discontinuities at all collocation points at time t. $\boldsymbol{\eta}$ is a diagonal matrix containing the components of the quasi-dynamics term for each collocation point.

In our implementation, the final elasto-static system (32) is written at all collocation points in the **local** Cartesian coordinate system $\boldsymbol{e}_1 = \boldsymbol{s}_1, \boldsymbol{e}_2 = \boldsymbol{s}_2, \boldsymbol{e}_3 = \boldsymbol{n}$ of each element. Such a choice reduces the computational burden as the constitutive relation of the interface is naturally expressed in such a coordinate system (see section 2.2. The global vector of displacement discontinuity is thus ordered as

$$\mathfrak{u} = \begin{bmatrix} \mathrm{u}_{s_1}^1 \\ \mathrm{u}_{s_2}^1 \\ \mathrm{u}_n^1 \\ \vdots \\ \mathrm{u}_{s_1}^j \\ \mathrm{u}_{s_2}^j \\ \mathrm{u}_n^j \\ \vdots \\ \mathrm{u}_{s_1}^{N_e} \\ \mathrm{u}_{s_2}^{N_e} \\ \mathrm{u}_n^{N_e} \end{bmatrix}$$

where N_e denotes the total number of collocation points in the mesh which is equal to the number of elements. The global vector of tractions is ordered similarly: $\boldsymbol{T} = [T_{s_1}^1, T_{s_2}^1, T_n^1, ..., T_{s_1}^i, T_{s_2}^i, T_n^i, ..., T_{s_1}^{N_e}, T_{s_2}^{N_e}, T_n^{N_e}]^T$. The elastic system (32) has $N_m = n_d \times N_e$ unknowns where n_d denotes the dimension of the problem (2 or 3).

We leverage hierarchical matrix algorithms to significantly speed up the solution of the dense linear system associated with the boundary element method while lowering the mmemory requirements. We refer to Hackbusch [2015] for details on the theory and alogrithms for hierarchical matrices. Our implementation follow closely the algorithm described in Chaillat et al. [2017]. The use of hierarchical matrix allows to lower the computation cost of the dot product $\mathbb{E} \cdot \mathfrak{u}$ from $\mathcal{O}(n^2)$ to $\mathcal{O}(n \log n)$ (as well as the memory requirement for the elastic operator). This is computationally attractive in conjunction with the use of an iterative solver for the solution of the jacobian system of the complete non-linear hydromechanical system as we discuss later on.

Introducing the effective tractions Before discussing the discretization of the fluid-flow inside the discontinuities, we rewrite the boundary element system discretizing the solid balance of momentum by adding and substracting the fluid pore pressure which acts on the normal direction to each element. We rewrite the previous equilibrium equation introducing Terzaghi's effective tractions $\boldsymbol{T}' = \boldsymbol{T} + p\boldsymbol{n}$. Because the pore pressure acts only in the local normal direction, the vector of effective tractions at the collocation poiints in the local frame of the boundary element is obtained as

$$\boldsymbol{T}' = \boldsymbol{T} + \mathbb{I}_n \cdot \boldsymbol{p}_{col}$$

where $\boldsymbol{p}_{col}$ is a vector of size N_e containing the pore-pressure at the location of the collocation points and $\mathbb{I}_n$ is a matrix of size $(n_d \times N_e) \times (N_e)$, ensuring that pore-pressure acts only on the normal component of the local traction, i.e.

$$\mathbb{I}_n = \begin{bmatrix} 0 & 0 & 0 & & \cdots & & & & \\ 0 & 0 & 0 & & \cdots & & & & \\ 1 & 0 & 0 & 0 & \cdots & 0 & 0 & 0 & \cdots \\ 0 & 0 & 0 & 0 & 0 & 0 & & & \\ 0 & 0 & 0 & 0 & 0 & 0 & & & \\ 0 & 1 & 0 & 0 & \cdots & 0 & 0 & 0 & \cdots \\ & & & & \vdots & & & & \\ \vdots & & & & & & & & \vdots \end{bmatrix},$$

Adding and substracting pore-pressure in the normal direction of each element, the time-derivative of the discretized elastostatic equilibrium (32) reduces to:

$$\dot{\boldsymbol{T}}' - \dot{\boldsymbol{T}}^o = \mathbb{E} \cdot \dot{\mathfrak{u}} + \mathbb{I}_n \cdot \dot{\boldsymbol{p}}_{col} - \boldsymbol{\eta}\ddot{\mathfrak{u}} \tag{33}$$

where a dot denotes a time-derivative. In the previous equation, $\dot{\boldsymbol{p}}_{col}$ is the rate of pore-pressure at the collocation points.

3.1.1 Elasto-plastic solver

Assuming for a moment that the rate of change of pore-pressure at the collocation points $\dot{\boldsymbol{p}}_{col}$ is known, we discuss the solution of the elastic system in combination with an elastoplastic interface law relating the interface effective tractions and the total displacement discontinuity. Such a non-linear system, when discretized is akin to a system of differential algebraic equations with inequality constraints.

We solve in a time-stepping manner from a known solution at time t^n to $t^n + \Delta t$ using a classical implicit integration scheme [Simo and Hughes, 1998, de Souza Neto et al., 2011]. Introducing the increment of total displacement discontinuity, effective tractions and internal variables:

$$\begin{aligned}\Delta \mathbf{u} &= \mathbf{u}^{n+1} - \mathbf{u}^n \\ \Delta \boldsymbol{T}' &= \boldsymbol{T}'^{n+1} - \boldsymbol{T}'^n \\ \Delta \boldsymbol{\chi} &= \boldsymbol{\chi}^{n+1} - \boldsymbol{\chi}^n\end{aligned}$$

we write the residuals of the mechanical problem in rate form (33) taking the increment of total displacement discontinuity $\Delta\mathbf{u}$ as the primary unknowns:

$$\boldsymbol{r}_m(\Delta \mathbf{u}) = \Delta \boldsymbol{T}'^{,o} - \Delta \boldsymbol{T}'(\Delta \mathbf{u}, \boldsymbol{\chi}^{n+1}, \boldsymbol{T}'^n) + \mathbb{E} \cdot \Delta \mathbf{u} + \mathbb{I}_n \cdot \Delta \boldsymbol{p} - \boldsymbol{\eta}\left(\Delta \mathbf{u} - \Delta \mathbf{u}^n\right)/\Delta t. \tag{34}$$

In this mechanical residual, we have highlighted the dependence of the increment of the interfaces effective tractions vector on the increment of displacement discontinuities $\Delta\mathbf{u}$, internal variables $\boldsymbol{\chi}^{n+1}$ and effective tractions at time t^n. We use a Newton-Raphson scheme to find the root of such a non-linear system of equations combined with an elastic predictor-corrector step to integrate locally the interface elasto-plastic law $\Delta \boldsymbol{T}'(\Delta \mathbf{u}, \boldsymbol{\chi}^{n+1}, \boldsymbol{T}'^n, \boldsymbol{t})$ [de Souza Neto et al., 2011]. The solution of the local interface constitutive relation previously described for a given increment of total displacement discontinuity $\Delta\mathbf{u}$ is detailed in appendix **??**.

At iteration k, the Newton-Raphson step reads (with $\boldsymbol{x} = \Delta\mathbf{u}$)

$$\begin{aligned}\mathbb{J}_m \delta \boldsymbol{x}^k &= -\boldsymbol{r}_m(\boldsymbol{x}^{k-1}) \\ \boldsymbol{x}^k &= \boldsymbol{x}^{k-1} + \alpha^k \delta \boldsymbol{x}^k\end{aligned}$$

where $\alpha^k = 1$ for a Newton step. Note that we use an inexact line-search in order to obtain α^k ensuring a good descent [Dennis Jr and Schnabel, 1996, Nocedal, J. and Wright, S. J., 2002]. The Jacobian of the mechanics equation $\mathbb{J}_m$ is

$$\mathbb{J}_m = \mathbb{E} - \mathbb{C}^{ep} \tag{35}$$

where

$$\mathbb{C}^{ep} = \frac{\mathrm{d}\Delta \boldsymbol{T}'}{\mathrm{d}\Delta \mathbf{u}} \tag{36}$$

contains the consistent tangent operator of the interface elasto-plastic law at all collocation points. It is therefore a block sparse matrix. We combine a convergence criteria on both the residual and on the sequence of $\boldsymbol{x}^k$. Similarly than for the solution of elastoplastic initial boundary value problems, the use of the exact expression of the consistent tangent operator is crucial to achieve robust convergence.

3.2 Fluid-flow in the discontinuities

We discretize the fluid volume balance (20) and Darcy's law (12) along the fractures/faults using a Galerkin finite element method using linear shape function for the pore-pressure. This choice notably allows to naturally handle fractures intersection as the fluid pressure will necessarily be continuous between elements. The weak form of equations (20)-(12) for an impermeable matrix is given by:

$$\int_\Gamma v \frac{\partial \mathrm{u}_n}{\partial t}\, \mathrm{d}S + \int_\Gamma v\, \frac{w}{M} \frac{\partial p}{\partial t}\, \mathrm{d}S + \int_\Gamma \boldsymbol{\nabla}_{||} v \cdot \left(\frac{w(\mathbf{u}) k(\mathbf{u})}{\mu_f} \right) \boldsymbol{\nabla}(p - p^o)\, \mathrm{d}S = \int_\Gamma v \times \gamma \mathrm{d}S \tag{37}$$

where v is a scalar test function with the same regularity than the pore pressure field. We have imposed zero fluid flux at the outer perimeter of the fractures, and assumed a quiescent initial state with an initially hydrostatic pore-pressure p^o.

The fracture mid-plane is discretized with finite elements (segments in 2D, triangle in 3D) with linear shape functions for simplicity. The pressure unknowns are thus at the vertex of the mesh. As the displacement discontinuity are discretized with a piece-wise discontinuous interpolation, $\mathfrak{u}_n$ is constant over the element. Moreover, the interface permeability is possibly non-linear as function of the normal displacement discontinuity $\mathfrak{u}_n$ and as such is assumed constant over the element. After finite element discretization and assembly, we obtain the following system of ordinary differential equations:

$$\mathbb{V} \cdot \dot{\mathbf{u}} + \mathbb{S}(\mathbf{u}) \cdot \dot{\boldsymbol{p}} + \mathbb{L}(\mathbf{u}) \cdot (\boldsymbol{p} - \boldsymbol{p}^o) = \boldsymbol{f}_f \tag{38}$$

where we have highlighted the *possible* dependence of the interfaces permeabilityand storage coefficient on the displacement discontinuity. These different finite element matrices at the element level for an element Γ_e with n_n nodes are given by:

$$\begin{aligned}
\mathbb{V}^e &= \int_{\Gamma_e} \boldsymbol{N}^T \cdot \mathbb{I}_n^e \, \mathrm{d}S \\
\mathbb{S}^e &= \int_{\Gamma_e} \frac{w}{M} \boldsymbol{N}^T \cdot \boldsymbol{N} \, \mathrm{d}S \\
\mathbb{L}^e &= \int_{\Gamma_e} \frac{w(\mathfrak{u}_n) k(\mathfrak{u}_n)}{\mu_f} \nabla \boldsymbol{N}^T \cdot \nabla \boldsymbol{N} \, \mathrm{d}S \\
\boldsymbol{f}_f^e &= \int_{\Gamma_e} \, \mathrm{d}S
\end{aligned}$$

where $\boldsymbol{N}$ and $\nabla \boldsymbol{N}$ are the matrices of shape functions and their spatial derivatives [Zienkiewicz et al., 2005]. $\mathbb{I}_{en}$ is a $n_n \times n_d$ sparse matrix (where n_d is the problem dimension) such that only the effect of the normal displacement is taken into account: $(\mathbb{I}_n^e)_{i3} = 1$, zero otherwise. The global finite element matrices for the whole mesh are obtained by classical assembly. We write these global matrices without the superscript e.

Like for the mechanical problem, we use an implicit time-integration scheme (backward Euler) to obtain the solution at $t^{n+1} = t^n + \Delta t$. The residual flow vector for equation (38) is given by:

$$\boldsymbol{r}_f(\Delta \boldsymbol{p}, \Delta \mathbf{u}) = \mathbb{V} \cdot \Delta \mathbf{u} + \left(\mathbb{S}(\mathbf{u}^{n+1}) + \Delta t \mathbb{L}(\mathbf{u}^{n+1}) \right) \cdot \Delta \boldsymbol{p} + \Delta t \mathbb{L}(\mathbf{u}^{n+1}) \cdot (\boldsymbol{p}^n - \boldsymbol{p}^o) - \Delta t \boldsymbol{f}_f \tag{39}$$

Note that in the case of constant permeability and storage, when the volume change of the interface is negligible, the flow problem uncouples from mechanics and becomes linear for the pressure increment.

3.3 A fully-coupled hydro-mechanical solver

In the scope of an implicit time-stepping scheme, the mechanics and flow residuals are given by eqs (34)-(39). Taking the increment of displacement discontinuity and pressure as main unknwons during the step, we obtain

$$\begin{aligned}
\boldsymbol{r}_m(\Delta \mathbf{u}, \Delta \boldsymbol{p}) &= \mathbb{E} \cdot \Delta \mathbf{u} - \Delta \boldsymbol{T}'(\Delta \mathbf{u}, \Delta \boldsymbol{\chi}) + \mathbb{N}_p \cdot \Delta \boldsymbol{p} + \Delta \boldsymbol{T}^o - \boldsymbol{\eta} \left(\Delta \mathbf{u} - \Delta \mathbf{u}^n \right) / \Delta t \\
\boldsymbol{r}_f(\Delta \mathbf{u}, \Delta \boldsymbol{p}) &= \mathbb{V} \cdot \Delta \mathbf{u} + \left(\mathbb{S}(\Delta \mathbf{u}) + \Delta t \mathbb{L}(\Delta \mathbf{u}) \right) \cdot \Delta \boldsymbol{p} + \Delta t \mathbb{L}(\Delta \mathbf{u}) \cdot \boldsymbol{p}^n - \Delta t \boldsymbol{f}_f
\end{aligned}$$

where the only difference lie in the appearance of matrix $\mathbb{N}_p$ in the mechanical residuals due to the fact that the pore-pressure are unknowns at the nodes while the mechanical equations are written at the collocation points of the boundary element method. This matrix $\mathbb{N}_p$ is highly sparse and as before acts only on the local normal boundary integral equation. For piece-wise constant displacement discontinuity element, the collocation point is located at the centroid of the element. As a result the non-zero entries of $\mathbb{N}_p$ are chiefly obtained. In fact, using an iterative solver for the solution of the tangent linear system, we do not even need to build this matrix (similarly for $\mathbb{V}$).

We find the root of $\mathbf{r} = \begin{bmatrix} \mathbf{r}_m \\ \mathbf{r}_f \end{bmatrix}$ via a Newton-Raphson scheme - where the unknowns are $\mathbf{X} = \begin{bmatrix} \boldsymbol{\Delta}\mathfrak{u} \\ \boldsymbol{\Delta}\mathbf{p} \end{bmatrix}$. At iteration k of this Newton-raphson scheme, we aim at:

$$\mathbf{r}(\mathbf{X}^{k+1}) = \mathbf{r}(\mathbf{X}^k) + (\nabla_{\mathbf{X}} \mathbf{r}(\mathbf{X}^k)) \cdot \delta \mathbf{X}^k = \mathbf{0}.$$

Using a line-search, we write the update as

$$\mathbf{X}^{k+1} = \mathbf{X}^k + \alpha^k \delta \mathbf{X}^k$$

where $\delta\mathbf{X}^k$ is the descent direction, solution of the linearized system

$$\mathbf{r}(\mathbf{X}^k) + (\nabla_{\mathbf{X}} \mathbf{r}(\mathbf{X}^k)) \cdot \delta \mathbf{X}^k = \mathbf{0}$$

i.e. the tangent system:

$$(\nabla_{\mathbf{X}} \mathbf{r}(\mathbf{X}^k)) \cdot \delta \mathbf{X}^k = -\mathbf{r}(\mathbf{X}^k)$$

We use an inexact wolfe line-search (to ensure that $\mathbf{r}^{k+1} < \mathbf{r}^k + ...$) as discussed in [Nocedal, J. and Wright, S. J., 2002, Dennis Jr and Schnabel, 1996]. We of course first try the Newton step $\alpha^k = 1$.

3.3.1 Solution of the Jacobian system

Using the notation of the previus sections, the Jacobian matrix of the coupled hydro-mechanical system has a block structure given by

$$\nabla_{\mathbf{X}} \mathbf{r}(\mathbf{X}^k) = \left[\begin{array}{cc} \mathbb{E} - \mathbb{C}^{ep} & \mathbb{N}_p \\ \mathbb{V} + (\nabla_{\Delta \mathfrak{u}} \mathbb{S} + \Delta t \nabla_{\Delta \mathfrak{u}} \mathbb{L}) \cdot \mathbf{\Delta p}^k & \mathbb{S} + \Delta t \mathbb{L} + \Delta t \left(\nabla_{\Delta p} \mathbb{L} \right) \cdot \mathbf{\Delta p}^k \end{array} \right]$$

where $\Delta t \left(\nabla_{\Delta p} \mathbb{L} \right) \cdot \mathbf{\Delta p}^k$ and $(\nabla_{\Delta \mathfrak{u}} \mathbb{S} + \Delta t \nabla_{\Delta \mathfrak{u}} \mathbb{L}) \cdot \mathbf{\Delta p}^k$ are consistent tangent operator for the flow problems, while $\mathbb{C}^{ep}$ is the elasto-plastic consistent tangent operator of the interface given by eq.(36).

The block of the Jacobian corresponding to the flow parts are obtained via differentiation of the corresponding part of the residual at the element level. Notably

$$\nabla_{\Delta \mathfrak{u}} \mathbb{S} \cdot \mathbf{\Delta p}$$

at the element level, for piece-wise constant displacement discontinuity element, ends up being a diagonal matrix (separating the terms coming from $\mathfrak{u}_n / M$ (i.e with a potential non-linearity of M):

$$\left(\int_{\Gamma_e} \boldsymbol{N}^T \frac{1}{M} \boldsymbol{N} \, \mathrm{d}S \right) \cdot \mathbf{\Delta p_e} + w_e \left(\int_{\Gamma_e} \boldsymbol{N}^T \frac{\partial (1/M)}{\partial \mathfrak{u}_n} \boldsymbol{N} \, \mathrm{d}S \right) \cdot \mathbf{\Delta p_e}$$

where $w_e = w_o + \mathfrak{u}_n$ is the current thickness of element e. Similarly

$$\nabla_{\Delta \mathfrak{u}} \mathbb{L} \cdot \mathbf{\Delta p}$$

is at the element level

$$\left(\int_{\Gamma_e} \frac{1}{\mu_f} \frac{\partial (w \times k)}{\partial \Delta \mathfrak{u}_n} \boldsymbol{\nabla} \boldsymbol{N}^T \cdot \boldsymbol{\nabla} \boldsymbol{N} \, \mathrm{d}S \right) \cdot \Delta p_e.$$

We can schematically rewrite the Jacobian matrix in 4 separate blocks, and write the system as:

$$\left[\begin{array}{cc} \mathbf{A}_{11} & \mathbf{A}_{12} \\ \mathbf{A}_{21} & \mathbf{A}_{22} \end{array} \right] \left[\begin{array}{c} \mathbf{x}_1 \\ \mathbf{x}_2 \end{array} \right] = \left[\begin{array}{c} \mathbf{b}_1 \\ \mathbf{b}_2 \end{array} \right]$$

with

$$\mathbf{A}_{11} = \mathbb{E} - \mathbb{C}^{ep} \qquad \mathbf{A}_{12} = \mathbb{N}_p$$
$$\mathbf{A}_{21} = \mathbb{V} + (\nabla_{\Delta \mathfrak{u}} \mathbb{S} + \Delta t \nabla_{\Delta \mathfrak{u}} \mathbb{L}) \cdot \mathbf{\Delta p}^k$$
$$\mathbf{A}_{22} = \mathbb{S} + \Delta t \mathbb{L} + \Delta t \left(\nabla_{\Delta p} \mathbb{L} \right) \cdot \mathbf{\Delta p}^k$$

we note that the flow blocks need to be updated at every iteration of the Newton-Raphson (as $\mathbb{L}$, $\mathbb{S}$ etc.) depends on opening (and possibly pressure).

In order to benefit from the hierarchical representation of the collocation boundary element matrix, we solve this Jacobian system of equations via an iterative method using a triangular pre-conditioner.

We use an upper block triangular pre-conditioner,

$$\mathbf{P}_{up} = \begin{bmatrix} \mathbf{A}_{11} & \mathbf{A}_{12} \\ \mathbf{0} & \tilde{\mathbf{S}} \end{bmatrix} \qquad \tilde{\mathbf{S}} = \mathbf{A}_{22} - \mathbf{A}_{21}\tilde{\mathbf{A}}_{11}^{-1}\mathbf{A}_{12}$$

where $\tilde{\mathbf{S}}$ is an approximation of the Schur complement and $\tilde{\mathbf{A}}_{11}$ an approximation of $\mathbf{A}_{11}$ for which we can "cheaply" compute an inverse . We then transform the original system

$$\mathbf{A} \cdot \mathbf{x} = \mathbf{b}$$

into

$$\left(\mathbf{A}\mathbf{P}_{up}^{-1}\right)\mathbf{u} = \mathbf{b}, \text{ and } \mathbf{P}_{up}\mathbf{x} = \mathbf{u},$$

where

$$\mathbf{P}_{up}^{-1} = \begin{bmatrix} \mathbf{A}_{11}^{-1} & -\mathbf{A}_{11}^{-1}\mathbf{A}_{12}\tilde{\mathbf{S}}^{-1} \\ \mathbf{0} & \tilde{\mathbf{S}}^{-1} \end{bmatrix}$$

The above system of equations is first solved for $\mathbf{u}$ by solving $\left(\mathbf{A}\mathbf{P}_{up}^{-1}\right)\mathbf{u} = \mathbf{b}$ using robust iterative solvers like GMRES. The application of the preconditioner in the above computation is akin to solving $\mathbf{P}_{up}\mathbf{z} = \mathbf{y}$, which we can rewrite as

$$\mathbf{z}_2 = \tilde{\mathbf{S}}^{-1} \cdot \mathbf{y}_2$$
$$\mathbf{A}_{11}\mathbf{z}_1 = \mathbf{y}_1 - \mathbf{A}_{12}\mathbf{z}_2$$

We therefore see that at each iteration of the iterative tangent solver, we need to solve a mechanical system. Unfortunately, using an approximation for $\mathbf{A}_{11}$ at the pre-conditioner level (for example a diagonal or an ILU decomposition of the near-diagonal term) is not robust when fracture opening occurs. We solve the $\mathbf{A}_{11}$ system using an iterative method such as BICGSTAB with a Jacobi pre-conditioner. We approximate the inverse of the approximated Schur complement with an ILU-T decomposition [Li, 2005]. Once we have calculated $\mathbf{u}$ using the above, we compute $\mathbf{x}$ by solving the $\mathbf{P}_{up}\mathbf{x} = \mathbf{u}$ which mimics the same steps as applying the preconditioner as explained above.

3.4 Adaptive time-stepping

Adaptive time-stepping for a system of ODEs requires an estimation of the local truncation error (LTE). This is not directly available for a fully implicit scheme. One can estimate such an LTE in a crude way by comparing a simple "explicit" prediction from the time-derivative estimated at the previous step and the solution of the non-linear implicit step (see Sheng et al. [2002], Diersch [2013] for details). Denoting $\boldsymbol{X}^n$ and $\dot{\boldsymbol{X}}^n$ the solution and rate at time t_n, and similarly $\boldsymbol{X}^n$ and $\dot{\boldsymbol{X}}^n$ at $t_n = t_{n-1} + \Delta t_n$. A first-order explicit extrapolation provides

$$\tilde{\boldsymbol{X}}_n = \boldsymbol{X}_{n-1} + \Delta t_n \dot{\boldsymbol{X}}_{n-1}$$

and a second-order accurate one

$$\boldsymbol{X}_n = \boldsymbol{X}_{n-1} + \Delta t_n \dot{\boldsymbol{X}}_{n-1} + \frac{1}{2}\Delta t_n^2 \boldsymbol{A}$$

where the acceleration can be estimated as

$$\boldsymbol{A} = \frac{\dot{\boldsymbol{X}}_n - \dot{\boldsymbol{X}}_{n-1}}{\Delta t_n}.$$

The LTE is estimated as time t_{n+1} as the norm of the difference between the first order and second order estimate [Kavetski et al., 2002]:

$$LTE(t_n) \approx e_n = \frac{\Delta t_n}{2}\|\dot{\boldsymbol{X}}_n - \dot{\boldsymbol{X}}_{n-1}\|.$$

It is worth recalling that the implicit scheme previously discussed solve for $\Delta\boldsymbol{X}$, in other word for the rate of change of the solution at t_{n+1}.

More specifically, to ensure a better scaling, we estimate one LTE for pressure and one for displacement discontinuity and scale it with the norm of the current solution:

$$e_{n+1}(\boldsymbol{p}) = \frac{\Delta t_n}{2} \|\dot{\boldsymbol{p}}^{n+1} - \dot{\boldsymbol{p}}^n\| / \|\boldsymbol{p}^{n+1}\| \qquad e_{n+1}(\boldsymbol{d}) = \frac{\Delta t_n}{2} \|\dot{\boldsymbol{d}}^{n+1} - \dot{\boldsymbol{d}}^n\| / \|\boldsymbol{d}^{n+1}\|$$

and takes the maximum of these two estimates to adapt the time step.

With such an LTE in hand, we use a PI controller as described in Söderlind [2002], Söderlind and Wang [2006] to adapt the time-step size for the subsequent step. Denoting Δt_{n+1}, this new time-step size,

$$\Delta t_{n+1} = \Delta t_n \times \left(\frac{\epsilon_{TOL}}{e_{n+1}}\right)^{3/5/1} \times \left(\frac{e_n}{\epsilon_{TOL}}\right)^{1/5/1}$$

In addition, one can enforce a minimum time-step size, and enforce a maximum factor M such that at most $\Delta t_{n+1} = M \Delta t_n$. To ensure $e_{n+1} \neq 0$, we add the square root of machine precision to the estimate of e_{n+1}.

References

O. Coussy. *Poromechanics*. Wiley, New-York, 2004.

J. Rice and M. Cleary. Some basic stress diffusion solutions for fluid-saturated elastic porous media with compressible constituents. *Rev. Geoph.*, 14(2):227–241, 1976.

E. Detournay and A.H.D. Cheng. Fundamentals of poroelasticity. In *Comprehensive Rock Engineering*. Pergamon Press, 1993.

Inga Berre, Florian Doster, and Eirik Keilegavlen. Flow in fractured porous media: A review of conceptual models and discretization approaches. *Transport in Porous Media*, 130(1):215–236, 2019.

Evgenii Kanin, Dmitry Garagash, and Andrei A Osiptsov. The near-tip region of a hydraulic fracture with pressure-dependent leak-off and leak-in. *J. Mech. Phys. Solids*, 2019.

Evgenii A Kanin, Egor V Dontsov, Dmitry I Garagash, and Andrei A Osiptsov. A radial hydraulic fracture with pressure-dependent leak-off. *Journal of the Mechanics and Physics of Solids*, 143:104062, 2020.

Antonio Gens, I Carol, and EE Alonso. A constitutive model for rock joints formulation and numerical implementation. *Computers and Geotechnics*, 9(1-2):3–20, 1990.

Ignacio Carol, Pere C Prat, and Carlos M Lopez. Normal/shear cracking model: application to discrete crack analysis. *Journal of engineering mechanics*, 123(8):765–773, 1997.

K. Park and G. H. Paulino. Cohesive zone models: a critical review of traction-separation relationships across fracture surfaces. *Applied Mechanics Reviews*, 64(6):060802, 2011.

Nick Barton. The shear strength of rock and rock joints. *International Journal of rock mechanics and mining sciences & Geomechanics abstracts*, 13(9):255–279, 1976.

N. Barton, S. Bandis, and K. Bakhtar. Strength, Deformation and Conductivity Coupling of Rock Joints. *Int. J. Rock. Mech. Min. Sci. & Geomech. Abstr.*, 22(3):121–140, 1985.

Z. Mroz and G. Giambanco. An interface model for analysis of deformation behaviour of discontinuities. *International Journal for Numerical and Analytical Methods in Geomechanics*, 20(1):1–33, 1996.

Stanislaw Stupkiewicz and Zenon Mroz. Modeling of friction and dilatancy effects at brittle interfaces for monotonic and cyclic loading. *Journal of Theoretical and Applied Mechanics*, 39:707–739, 2001.

B.-K. Son, Y.-K. Lee, and C.-I. Lee. Elasto-plastic simulation of a direct shear test on rough rock joints. *International Journal of Rock Mechanics and Mining Sciences*, 41(SUPPL. 1):2A 07 1–6, 2004. doi: 10.1016/j.ijrmms.2004.03.066.

M.T. Zandarin, E. Alonso, and S. Olivella. A constitutive law for rock joints considering the effects of suction and roughness on strength parameters. *International Journal of Rock Mechanics and Mining Sciences*, 60: 333–344, 2013. doi: 10.1016/j.ijrmms.2012.12.007.

Y. Li, J. Oh, R. Mitra, and B. Hebblewhite. A constitutive model for a laboratory rock joint with multi-scale asperity degradation. *Computers and Geotechnics*, 72:143–151, 2016. doi: 10.1016/j.compgeo.2015.10.008.

Y. Li, W. Wu, and X. Wei. Analytical modeling of the shear behavior of rock joints with two-order asperity dilation and degradation. *International Journal of Geomechanics*, 20(6), 2020. doi: 10.1061/(ASCE)GM.1943-5622.0001645.

SC Bandis, AC Lumsden, and NR Barton. Fundamentals of rock joint deformation. In *International Journal of Rock Mechanics and Mining Sciences & Geomechanics Abstracts*, volume 20, pages 249–268. Elsevier, 1983.

J. Rutqvist and O. Stephansson. The role of hydrochemical coupling in fractured rock engineering. *Hydrogeology Journal*, 11(1):7–40, 2003.

BNJ Persson. Relation between interfacial separation and load: a general theory of contact mechanics. *Physical review letters*, 99(12):125502, 2007.

James Kenneth Mitchell, Kenichi Soga, et al. *Fundamentals of soil behavior*, volume 3. John Wiley & Sons New York, 2005.

F. H. Cornet. *Elements of Crustal Geomechanics.* Cambridge University Press, 2015.

Itasca Consulting Group. FLAC Constitutive models. Technical report, Itasca Consulting Group, 2010.

J. R. Rice. Fault stress states, pore pressure distributions, and the weakeness of the san andreas fault. *International Geophysics*, 51(Fault Mechanics and Transport Properties of Rock: A Festschrift in Honor of W. F. Brace):475–503, 1992.

P. A. Witherspoon, J. S.Y. Wang, K. Iwai, and J. E. Gale. Validity of cubic law for fluid flow in a deformable rock fracture. *Water Resources Res.*, 16(6):1016–1024, 1980.

S. L. Crouch and A. M. Starfield. *Boundary element methods in solid mechanics.* George Allen & Unwin, 1983.

D. A. Hills, P. A. Kelly, D. N. Dai, and A. M. Korsunsky. *Solution of crack problems: the distributed dislocation technique*, volume 44 of *Solid Mechanics and its Applications.* Kluwer Academic Publ., Dordrecht, 1996.

M. Bonnet. *Boundary integral equation methods for solids and fluids.* John Wiley & Sons, 1999.

S. G. Mogilevskaya. Lost in translation: Crack problems in different languages. *International Journal of Solids and Structures*, 51(25):4492–4503, 2014.

S Nintcheu Fata. Explicit expressions for three-dimensional boundary integrals in linear elasticity. *Journal of computational and applied mathematics*, 235(15):4480–4495, 2011.

D. V. Nikolskiy, S. G. Mogilevskaya, and J. F. Labuz. Boundary element analysis of non-planar three-dimensional cracks using complex variables. *International Journal of Rock Mechanics and Mining Sciences*, 76:44–54, 2015.

J. R. Rice. Spatio-temporal complexity of slip on a fault. *Journal of Geophysical Research*, 98(B6):9885–9907, June 1993.

Wolfgang Hackbusch. *Hierarchical matrices: algorithms and analysis*, volume 49. Springer, 2015.

Stéphanie Chaillat, Luca Desiderio, and Patrick Ciarlet. Theory and implementation of h-matrix based iterative and direct solvers for helmholtz and elastodynamic oscillatory kernels. *Journal of Computational Physics*, 351:165–186, 2017.

J. C. Simo and T. J. R. Hughes. *Computational Inelasticity*. Springer, 1998.

Eduardo A. de Souza Neto, Djordje Peric, and David R.J. Owen. *Computational methods for plasticity: theory and applications*. John Wiley & Sons, 2011.

John E Dennis Jr and Robert B Schnabel. *Numerical methods for unconstrained optimization and nonlinear equations*. SIAM, 1996.

Nocedal, J. and Wright, S. J. *Numerical Optimization*. Springer, 2002.

Olek C Zienkiewicz, Robert Leroy Taylor, and Jian Z Zhu. *The finite element method: its basis and fundamentals*. Elsevier, 2005.

Xiaoye S Li. An overview of superlu: Algorithms, implementation, and user interface. *ACM Transactions on Mathematical Software (TOMS)*, 31(3):302–325, 2005.

Daichao Sheng, Scott W Sloan, and Andrew J Abbo. An automatic newton-raphson scheme. *International Journal of Geomechanics*, 2(4):471–502, 2002.

Hans-Jörg G Diersch. *FEFLOW: finite element modeling of flow, mass and heat transport in porous and fractured media*. Springer Science & Business Media, 2013.

Dmitri Kavetski, Philip Binning, and Scott W Sloan. Adaptive backward euler time stepping with truncation error control for numerical modelling of unsaturated fluid flow. *International Journal for Numerical Methods in Engineering*, 53(6):1301–1322, 2002.

Gustaf Söderlind. Automatic control and adaptive time-stepping. *Numerical Algorithms*, 31(1-4):281–310, 2002.

Gustaf Söderlind and Lina Wang. Adaptive time-stepping and computational stability. *Journal of Computational and Applied Mathematics*, 185(2):225–243, 2006.

A Integration of the interface law

Note: For clarity, in that section, we drop the $'$ from $\boldsymbol{T}'$, and use $\boldsymbol{T}$ - tractions implicitely refer to the effective tractions $\boldsymbol{T}'$.

The integration of the constitutive relation at the local level is performed for a given increment of displacement discontinuity

$$\Delta \mathbf{u}$$

in a fully implicit way. Such increment of displacement discontinuity is obtained from the iterative solution of the global momentum balance which is solved iteratively using a Newton-Raphson algorithm.

The algorithm marches in time from t^n to $t^n + \Delta t$. For a given $\Delta \boldsymbol{d}$, we seek the corresponding tractions, plastic/elastic DDs split and new internal variables at the end of the load step at t^{n+1} . We thus write

$$\begin{aligned}
\boldsymbol{T}^{n+1} &= \boldsymbol{T}^n + \Delta \boldsymbol{T} \\
\mathbf{u}^{n+1,p} &= \mathbf{u}^{n,p} + \Delta \mathbf{u}^p \\
\boldsymbol{\chi}^{n+1} &= \boldsymbol{\chi}^n + \Delta \boldsymbol{\chi} \\
&\ldots
\end{aligned}$$

In the following, we first recall the integration of the interface constitutive law when frictional failure occurs. The case of tensile failure, the choice of the mode of failure and the treatment of the contact condition upon interface opening are then briefly discussed.

A.1 Elastic predictor / plastic corrector scheme for a Mohr-Coulomb interface

A.1.1 Trial elastic state

First we assume a solely elastic step, often refeered to as the trial elastic state $\Delta \mathbf{u}^{e,*} = \Delta \mathbf{u}$ - using a $*$ superscript, we write the trial elastic state:

$$\begin{aligned}
\boldsymbol{T}^{*,n+1} &= \boldsymbol{T}^n + \mathbb{C} \cdot \Delta \mathbf{u} \qquad \Delta \boldsymbol{T}^* = \mathbb{C} \cdot \Delta \boldsymbol{d} \\
\boldsymbol{\chi}^{*,n+1} &= \boldsymbol{\chi}^n \qquad \Delta \boldsymbol{\chi}^* = \mathbf{0} \\
\Delta \lambda^* &= 0
\end{aligned}$$

. Note that in the case where the interface elastic normal stiffness K_n is evolving non-linear with normal traction, a proper non-linear integration is required to obtain the elastic trial state - which was written above for the simple case of constant stiffnesses.

The frictional yield function is then checked.

- If $F(\boldsymbol{T}^{*,n+1}, \boldsymbol{\chi}^n) < 0$, the step is indeed purely elastic

$$\begin{aligned}
\Delta \mathbf{u}^e &= \Delta \mathbf{u} \\
\boldsymbol{T}^{n+1} &= \boldsymbol{T}^{*,n+1} \\
\boldsymbol{\chi}^{n+1} &= \boldsymbol{\chi}^n
\end{aligned}$$

- if $F(\boldsymbol{T}^{*,n+1}, \boldsymbol{\chi}^n) > 0$, the step is elasto-plastic, and we must return the tractions back to the yield surface, and solve for the corresponding plastic multiplier increment during the step $\Delta \lambda$.

A.1.2 Plastic correction

First, we write the flow rule in an incremental way

$$\Delta \mathbf{u}^p = \Delta \lambda \times \boldsymbol{\nabla}_{\boldsymbol{T}^{n+1}} G = \Delta \lambda \left(\hat{\boldsymbol{s}}^{n+1} + \psi(\lambda^n + \Delta \lambda) \boldsymbol{n} \right)$$

where we have used the expression of the non-associated Mohr-Coulomb plastic potential. Note that we therefore deduce that, the plastic shear slip vector increment is:

$$\Delta \hat{\mathbf{u}}^p = \Delta \mathrm{u}^p_{s_1} \boldsymbol{s}_1 + \Delta \mathrm{u}^p_{s_2} \boldsymbol{s}_2 = \Delta \lambda \hat{\boldsymbol{s}}^{n+1} = \Delta \lambda \frac{\boldsymbol{\tau}^{n+1}}{\|\boldsymbol{\tau}^{n+1}\|}$$

We write the elastic relation as

$$\boldsymbol{T}^{n+1} = \boldsymbol{T}^n + \Delta\boldsymbol{T}^* - \mathbb{C}\cdot\Delta\mathbf{u}^p$$

or similarly

$$\Delta\boldsymbol{T} = \Delta\boldsymbol{T}^* - \mathbb{C}\cdot\Delta\mathbf{u}^p$$

We can now explicit the tractions at $\boldsymbol{T}^{n+1}$, notably the shear traction vector reads

$$\boldsymbol{\tau}^{n+1} = \boldsymbol{\tau}^n + \Delta\boldsymbol{\tau}^* - K_s\Delta\hat{\mathbf{u}}^p = \boldsymbol{\tau}^n + \Delta\boldsymbol{\tau}^* - K_s\Delta\lambda\hat{\boldsymbol{s}}^{n+1}$$

which we can further re-write as

$$\boldsymbol{\tau}^{n+1} = \boldsymbol{\tau}^* - K_s\Delta\lambda\frac{\boldsymbol{\tau}^{n+1}}{\|\boldsymbol{\tau}^{n+1}\|}$$

such that we can re-express the trial elastic state shear vector as

$$\boldsymbol{\tau}^* = \left(\|\boldsymbol{\tau}^{n+1}\| + K_s\Delta\lambda\right)\hat{\boldsymbol{s}}^{n+1}$$

Because $\hat{\boldsymbol{s}} = \boldsymbol{\tau}/\|\boldsymbol{\tau}\|$ is an unit vector, we thus have the relation

$$\frac{\boldsymbol{\tau}^*}{\|\boldsymbol{\tau}^*\|} = \hat{\boldsymbol{s}}^{n+1} = \frac{\boldsymbol{\tau}^{n+1}}{\|\boldsymbol{\tau}^{n+1}\|}$$

in other words, the trial elastic state directly provide the principal shear traction direction. This is always the case as long as the shear stiffness K_s is constant. Note also that it implies $\boldsymbol{\nabla}_{\boldsymbol{T}}\hat{s} = \boldsymbol{0}$. This is due to the circular shape of the yield function in the plane (T_{s_1}, T_{s_2}).

Plastic correction

We detail the case for a constant normal and shear stiffness. The case of a non-linear normal stiffness K_n (function of the normal traction) is chiefly obtained by a proper integration of the (then) non-linear elastic law ($\Delta\boldsymbol{T} = \mathbb{C}(T_n)\cdot\Delta\mathfrak{u}^e$).

We need to enforce the yield function at the end of the step - in other words:

$$F_{mc}(\boldsymbol{T}^{n+1}, \boldsymbol{\chi}^{n+1}) = 0$$

as well as the elastic constitutive increment

$$\Delta\boldsymbol{T} + \mathbb{C}\cdot\Delta\mathbf{u}^p = \Delta\boldsymbol{T}^* = \mathbb{C}\cdot\Delta\boldsymbol{d} \qquad \Delta\boldsymbol{T} = \Delta\boldsymbol{T}^* - \mathbb{C}\cdot\Delta\mathbf{u}^p$$
$$\Delta\mathbf{u}^p = \Delta\lambda\left(\hat{\boldsymbol{s}}^{n+1} + \psi(\lambda^n + \Delta\lambda)\boldsymbol{n}\right)$$

Note again that if the normal stiffness K_n is evolving non-linear with normal traction, proper integration of the non-linear elastic law is needed (the previous equation is valid for constant stiffness). The evolution of the hardening variables are here -

$$\Delta\chi_f = \Delta\lambda \qquad \Delta\chi_c = \Delta\lambda(1 + \psi(\lambda^n + \Delta\lambda))$$

We can rewrite the yield condition for the Mohr-Coulomb as function of the trial state and the increment of plastic strain

$$\boldsymbol{T}^*\cdot\hat{\boldsymbol{s}}^{n+1} + f(\lambda^n + \Delta\lambda)\boldsymbol{T}^*\cdot\boldsymbol{n} - c(\chi_c^n + \Delta\chi_c) = \mathbb{C}\cdot\Delta\mathbf{u}^p\cdot\hat{\boldsymbol{s}}^{n+1} + f(\lambda^n + \Delta\lambda)\mathbb{C}\cdot\Delta\mathbf{u}^p\cdot\boldsymbol{n}$$

where we recall that $\hat{s}^{n+1}$ is the shear traction direction (unit vector) directly given by the shear component of the trial elastic state $\boldsymbol{T}^*$.

Using the plastic flow rule, we obtain the following non-linear equation for the increment of the plastic multiplier

$$\boldsymbol{T}^*\cdot\hat{\boldsymbol{s}}^{n+1} + f(\lambda^n + \Delta\lambda)\boldsymbol{T}^*\cdot\boldsymbol{n} - c(\chi_c^n + \Delta\chi_c) = \left(K_s + K_n f(\lambda^n + \Delta\lambda)\psi(\lambda^n + \Delta\lambda)\right)\Delta\lambda \tag{40}$$

such that the plastic multiplier is solution of

$$\Delta\lambda = \frac{\boldsymbol{T}^{*} \cdot \hat{\boldsymbol{s}}^{n+1} + f(\lambda^n + \Delta\lambda)\boldsymbol{T}^{*} \cdot \boldsymbol{n} - c(\chi_c^n + \Delta\lambda(1 + \psi(\lambda^n + \Delta\lambda)))}{(K_s + K_n f(\lambda^n + \Delta\lambda)\psi(\lambda^n + \Delta\lambda))}$$

which can be solved numerically by any root-finding scheme (Newton etc.) or via fixed-point iterations.

Note that for constant friction / dilatancy / cohesion, the solution is directly obtained analytically in one-step.

$$\Delta\lambda = \frac{\boldsymbol{T}^{*} \cdot \hat{\boldsymbol{s}}^{n+1} + f\boldsymbol{T}^{*} \cdot \boldsymbol{n} - c}{(K_s + K_n f\psi)}$$

Once the increment of plastic multiplier is obtained, the new plastic strain, hardening variables and tractions at the end of the step ($t^n + \Delta t$) are chiefly obtained.

A.2 Consistent tangent operator

Note that the complete elasto-plastic integration algorithm can be schematically written as

$$\Delta\boldsymbol{T}(\Delta\mathbf{u}, \boldsymbol{T}^n, \boldsymbol{\chi}^n)$$

In other words, it provides the new traction $\boldsymbol{T}^n + \Delta\boldsymbol{T}$ from a given known increment of displacement $\Delta\mathbf{u}$ and value of the hardening variable at the beginning of the step. It defines an algorithmic incremental constitutive function

$$\boldsymbol{T}^{n+1} = \boldsymbol{T}^n + \Delta\tilde{\boldsymbol{T}}(\boldsymbol{\chi}^n, \mathbf{u}^n + \Delta\mathbf{u}) = \tilde{\boldsymbol{T}}(\boldsymbol{\chi}^n, \mathbf{u}^{n+1})$$

Within a load/time-step $[t^n, t^{n+1}]$, the set of internal variables $\boldsymbol{\chi}^n$ given as argument of $\tilde{\boldsymbol{T}}$ is *fixed*. Only the guess $\Delta\boldsymbol{d}$ changes during the global Newton-Raphson solution of the global balance of momentum (not $\boldsymbol{\chi}^n$). The function $\tilde{\boldsymbol{T}}$ defines a stress/strain relation within the interval $[t^n, t^{n+1}]$ equivalent to a non-linear elastic law. The consistent tangent modulus (or operator) is defined as the derivative of this constitutive law:

$$\mathbb{C}^{ep} = \frac{\mathrm{d}\Delta\boldsymbol{T}}{\mathrm{d}\Delta\mathbf{u}} = \frac{\partial\Delta\tilde{\boldsymbol{T}}}{\partial\Delta\mathbf{u}}|_{\boldsymbol{\chi}^n}$$

the derivative of $\tilde{T}$ with χ^n held constant. Such an operator can either be obtained numerically by finite difference

$$\mathbb{C}^{ep} \approx \frac{\Delta\tilde{\boldsymbol{T}}(\boldsymbol{\chi}^n, \Delta\mathbf{u}(1+\omega)) - \Delta\tilde{\boldsymbol{T}}(\boldsymbol{\chi}^n, \Delta\mathbf{u})}{\omega\Delta\mathbf{u}}$$

or via a consistent linearization of the previous elastic predictor / plastic corrector algorithm.

A.2.1 Consistent linearization

Linearization of the elasto-plastic law yields (for the case of constant stiffness)

$$\mathrm{d}\Delta\boldsymbol{T}^{n+1} = \mathbb{C} \cdot \left(\mathrm{d}\Delta\mathbf{u} - \frac{\partial\Delta\mathbf{u}^p}{\partial\Delta\mathbf{u}}\mathrm{d}\Delta\mathbf{u}\right)$$

A.2.2 In 2D

$$\mathbb{C}^{ep} = \begin{bmatrix} K_s\left(1 - \frac{K_s}{\theta^{n+1}}\right) & \frac{-K_n K_s \hat{s} f^{n+1}}{\theta^{n+1}} \\ \frac{-K_n K_s \hat{s} \times \psi^{n+1}}{\theta^{n+1}} & \frac{K_n\left(K_s - T_n^{n+1} f'^{n+1}\right)}{\theta^{n+1}} \end{bmatrix}$$

with

$$\theta^{n+1} = K_s + c'^{n+1} - T_n^{n+1} f'^{n+1} + K_n f^{n+1} \times \psi^{n+1}$$

and $\hat{s}$ in 2D is a scalar indicating the sign of the trial shear traction:

$$\hat{s} = \frac{T_s^*}{|T_s^*|} = \mathrm{sign}(T_s^*)$$

A.2.3 In 3D

For constant friction/dilatancy: Without softening (constant friction case)

$$\mathbb{C}^{ep} = \begin{bmatrix} K_s\left(1-\dfrac{K_s\left(\hat{\boldsymbol{s}}\cdot\boldsymbol{s}_1\right)^2}{\theta}\right) & \dfrac{-K_s^2\left(\hat{\boldsymbol{s}}\cdot\boldsymbol{s}_1\right)\left(\hat{\boldsymbol{s}}\cdot\boldsymbol{s}_2\right)}{\theta} & -\dfrac{K_nK_s\left(\hat{\boldsymbol{s}}\cdot\boldsymbol{s}_1\right)f}{\theta} \\ \dfrac{-K_s^2\left(\hat{\boldsymbol{s}}\cdot\boldsymbol{s}_1\right)\left(\hat{\boldsymbol{s}}\cdot\boldsymbol{s}_2\right)}{\theta} & K_s\left(1-\dfrac{K_s\left(\hat{\boldsymbol{s}}\cdot\boldsymbol{s}_2\right)^2}{\theta}\right) & -\dfrac{K_nK_s\left(\hat{\boldsymbol{s}}\cdot\boldsymbol{s}_2\right)f}{\theta} \\ -\dfrac{K_nK_s\left(\hat{\boldsymbol{s}}\cdot\boldsymbol{s}_1\right)\psi}{\theta} & -\dfrac{K_nK_s\left(\hat{\boldsymbol{s}}\cdot\boldsymbol{s}_2\right)\psi}{\theta} & \dfrac{K_nK_s}{\theta} \end{bmatrix}$$

with

$$\theta = K_s + K_n f\psi$$

With weakening of friction/dilatancy

$$\mathbb{C}^{ep} = \mathbb{C}^{ep} = \begin{bmatrix} c_{11}^{ep} & c_{12}^{ep} & -\dfrac{K_nK_s\left(\hat{\boldsymbol{s}}\cdot\boldsymbol{s}_1\right)f}{\theta^{n+1}} \\ c_{21}^{ep}=c_{12}^{ep} & c_{22}^{ep} & -\dfrac{K_nK_s\left(\hat{\boldsymbol{s}}\cdot\boldsymbol{s}_2\right)f}{\theta^{n+1}} \\ -\dfrac{K_nK_s\left(\hat{\boldsymbol{s}}\cdot\boldsymbol{s}_1\right)\psi^{n+1}}{\theta^{n+1}} & -\dfrac{K_nK_s\left(\hat{\boldsymbol{s}}\cdot\boldsymbol{s}_2\right)\psi^{n+1}}{\theta^{n+1}} & \dfrac{K_n\left(K_s - T_n^{n+1}f'^{n+1}\right)}{\theta^{n+1}} \end{bmatrix}$$

with

$$\begin{aligned} c_{11}^{ep} &= \frac{K_s\left(K_s\left(\boldsymbol{T}^{n+1}\cdot\boldsymbol{s}_2\right)^2\|\boldsymbol{\tau}^{n+1}\| + \left(K_s\left(\boldsymbol{T}^{n+1}\cdot\boldsymbol{s}_1\right)^2\Delta\lambda + \|\boldsymbol{\tau}^{n+1}\|^3\right)\gamma^{n+1}\right)}{\theta^{n+1}\alpha^{n+1}\|\boldsymbol{\tau}^{n+1}\|^2\left(K_s\Delta\lambda + \|\boldsymbol{\tau}^{n+1}\|\right)} \\ c_{22}^{ep} &= \frac{K_s\left(K_s\left(\boldsymbol{T}^{n+1}\cdot\boldsymbol{s}_1\right)^2\|\boldsymbol{\tau}^{n+1}\| + \left(K_s\left(\boldsymbol{T}^{n+1}\cdot\boldsymbol{s}_2\right)^2\Delta\lambda + \|\boldsymbol{\tau}^{n+1}\|^3\right)\gamma^{n+1}\right)}{\theta^{n+1}\alpha^{n+1}\|\boldsymbol{\tau}^{n+1}\|^2\left(K_s\Delta\lambda + \|\boldsymbol{\tau}^{n+1}\|\right)} \\ c_{21}^{ep} = c_{12}^{ep} &= -\frac{K_s^2\left(\hat{\boldsymbol{s}}\cdot\boldsymbol{s}_1\right)\left(\hat{\boldsymbol{s}}\cdot\boldsymbol{s}_2\right)\beta^{n+1}}{\theta^{n+1}\alpha^{n+1}} \end{aligned}$$

and

$$\begin{aligned} \theta^{n+1} &= K_s + c'^{n+1} - T_n^{n+1}f'^{n+1} + K_n f^{n+1}\times\left(\psi^{n+1}\right) \\ \alpha^{n+1} &= \boldsymbol{T}^{n+1}\cdot\hat{\boldsymbol{s}}^{n+1} \\ \beta^{n+1} &= \boldsymbol{T}^{n+1}\cdot\hat{\boldsymbol{s}}^{n+1} \\ \gamma^{n+1} &= \left(c'^{n+1} - T_n^{n+1}f'^{n+1} + K_n f^{n+1}\times\left(\psi^{n+1}\right)\right) \\ \boldsymbol{T}^{n+1}\cdot\hat{\boldsymbol{s}}^{n+1} &= \|\boldsymbol{\tau}^{n+1}\| \end{aligned}$$

A.3 Tensile failure

The elastic predictor - plastic corrector scheme is strictly similar than for the case of frictional failure. If after the estimation of the trial elastic state, tensile failure is activated, the plastic correction is obtained by solving, the non-linear system:

$$F_t(\boldsymbol{T}', \boldsymbol{\chi}) = 0$$

Note that when the tensile strength reduces to zero, the correction is trivial: $\Delta\mathbf{u}^p = \Delta\mathbf{u}$.